ACS OMEGA

Open Access

http://pubs.acs.org/journal/acsodf

Article

Theoretical Perspective toward Designing of 5-Methylbenzo [1,2-*b*:3,4-*b*′:6,5-*b*″] trithiophene-Based Nonlinear Optical Compounds with Extended Acceptors

Iqra Shafiq, Ayesha Mustafa, Romaisa Zahid, Rabia Baby, Sarfraz Ahmed, Muhammad Adnan Asghar,* Tansir Ahamad, Manawwer Alam, Ataualpa A. C. Braga, and Suvash Chandra Ojha*

Cite This: *ACS Omega* 2023, 8, 39288−39302

Read Online

ACCESS | Metrics & More | Article Recommendations | Supporting Information

ABSTRACT: A series of benzotrithiophene-based compounds (**DCTM1-DCTM6**) having D_1-π_1-D_2-π_2-A configuration were designed using a reference molecule (**DCTMR**) via incorporating pyrrole rings (n = 1−5) as the π-spacer (π_2). Quantum chemical calculations were performed to determine the impact of the pyrrole ring on the nonlinear optical (NLO) behavior of the above-mentioned chromophores. The optoelectronic properties of the compounds were determined at the MW1PW91/6-311G(d,p) functional. Among all of the derivatives, **DCTM5** exhibited the least highest occupied molecular orbital−lowest unoccupied molecular orbital (HOMO−LUMO) band gap (E_g) 0.968 eV with a high softness of 0.562 eV^{-1}, and hence possessed the highest polarizability. Interestingly, transition density matrix (TDM) findings demonstrated that **DCTM5** with an effective diagonal charge transmission proportion at the acceptor group supports the frontier molecular orbital (FMO) results. Additionally, the exciton binding energy values for **DCTM1-DCTM6** were found to be less than that for **DCTMR** and thus, the effective charge transfer was examined in the derivatives. All of the derivatives exhibited effective NLO outcomes with the highest magnitude of linear polarizability $\langle\alpha\rangle$, and first (β_{tot}) and second (γ_{tot}) hyperpolarizabilities relative to the parent compound. Nevertheless, the highest β_{tot} and γ_{tot} were obtained for **DTCM1** and **DTCM6**, 7.0440 × 10^{-27} and 22.260 × 10^{-34} esu, respectively. Hence, through this structural tailoring with a pyrrole spacer, effective NLO materials can be obtained for optoelectronic applications.

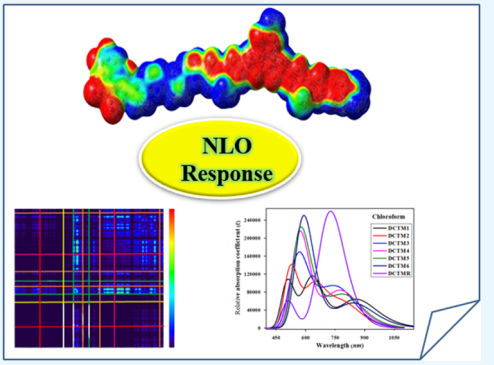

INTRODUCTION

For the past several decades, the most challenging task in research fields has been the development of advanced materials to produce distinct nonlinear optical (NLO) responses. The fields of optical computing, telecommunications,[1] electronics,[2] laser technology,[3] optoelectronics,[4] and photonic devices[5] all greatly benefit from these materials.[6] Several strategies have been used to create novel as well as enhanced materials that have outstanding NLO responses.[7,8] Organic as well as inorganic semiconductors, molecular dyes, nanomaterials, and organometallic compounds[9,10] are a few examples of these kinds of polymer frameworks. Concerning the applications of nonlinearity, each class has its own benefits and drawbacks. The research of nonlinear optics was first concentrated on solid inorganic materials like $LiNbO_3$ and KH_2PO_4, but for a variety of reasons, the attention progressively switched to organometallic and organic systems.[11] Due to their high electronic charge transfer (CT), and excitations at low energies, the transition organometallic complexes also functioned as possible constituents of second-order NLO materials.[12] New organic NLO active compounds have earned reputation as being advantageous for simulation analysis owing to their appealing structural characteristics such as quick reaction times, increased hyperpolarizability, affordability, higher band gaps, and the ability to be modulated structurally to produce a high NLO response.[13] Moreover, they exhibit exceptional optical transparency, natural softness, and outstanding stability in the visible spectrum. Moreover, organic compounds have a strong NLO response because of the adaptability of their chemical composition owing to various functional groups and a broad range of synthesis techniques. These unique structural characteristics account for their widespread use in several optical applications, including electro-optic switching modulation, frequency doubling, and the generation of terahertz (THz) waves.[14,15] In organic chromophores, powerful donor and acceptor groups are linked through the conjugated π-system, which in turn leads to the fast intramolecular charge transfer (ICT) that supports NLO

Received: July 4, 2023
Accepted: September 27, 2023
Published: October 12, 2023

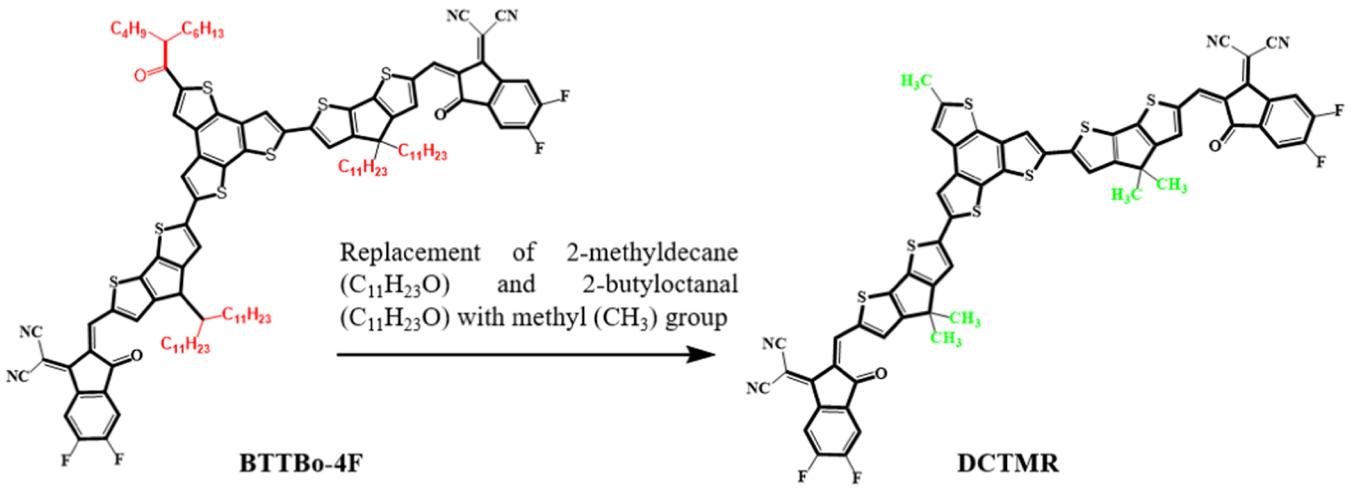

Figure 1. Alteration of **BTTBo-4F** to **DCTMR** by replacing the bulky groups with the $-CH_3$ group.

characteristics.[16] Efficient D-π−A compounds can be designed by adjusting the structure of a push−pull scheme and assessing the impact of donor−acceptor (D−A) units.[17] Structural modeling is a crucial factor for NLO properties.[18]

The nonfullerene-based NLO compounds have been reported recently as efficient NLO materials and are now receiving attention owing to their unique properties, including less cost of production, fine-tunability, high molar extinction coefficients, ease of purification, and high absorption ranges in the near-infrared (NIR) and visible regions.[19−21] Moreover, NFAs' π-conjugation offers significant CT at the D−A contact, which helps with electronic delocalization.[22] Three thiophene groups fuse to the benzene core to produce the powerful electron-donating compound known as benzotrithiophene (BTT), which is currently recognized as an efficient donor that is substantially employed to improve NLO behavior. BTT's stiff, steric-hindrance-free molecular core makes it an ideal coplanar skeleton for NFEAs, allowing it to demonstrate many advantages.[23] Inter- and intramolecular bonds between D−A parts can induce self-assembly into organized frameworks and robust π-assembly of polymeric chains; these two factors aid in charge transition. Typical donor moieties arise from electron-donating materials such as benzo[1,2-*b*:4,5-*b*′]-dithiophene, cyclopenta[2,1-*b*:3,4-*b*′]dithiophene, dithieno-[3,2-*b*:2′,3′-*d*]silole, and dithieno[3,2-*b*:2′,3′-*d*]pyrrole, which have been copolymerized via powerful 'A' like 2,1,3-benzothiadiazole (BTZ) to develop efficient organic semiconductors for electronic devices.[24−27] Adding an acyl electron-withdrawing group to BTT may improve energy levels, solubility, and intramolecular push−pull interactions to increase the near-infrared absorption. Moreover, BTT's asymmetrical distribution of the electronic cloud enhances the exciton dissociation efficiency and boosts the dipole moment. Because of its outstanding characteristics, BTT has become a viable option for building high-performance NLO materials.[28,29]

Therefore, keeping in view the previous discussion, in this study we have chosen an organic fullerene free BTT-based synthesized parent compound, namely 2,2′-((2*Z*,2′*Z*)-((6,6′-(5-(2-butyloctanoyl)benzo[1,2-*b*:3,4-*b*′:6,5-*b*″]trithiophene-2,8-diyl)bis(4,4-bis(2-butyloctyl)-4*H*-cyclopenta[1,2-*b*:5,4-*b*′]-dithiophene-6,2-diyl))bis(methanylylidene))bis(5,6-difluoro-3-oxo-2,3-dihydro-1*H*-indene-2,1-diylidene))dimalononitrile (**BTTBo-4F**)[30] comprising the A-π-D-π−A framework. Further, in the parent compound (**BTTBo-4F**), the bulky groups, i.e., 2-methyldecane and 2-butyloctanal, attached to the π-spacer and donor are substituted by methyl ($-CH_3$) to lessen the computational cost and to avoid steric hindrance due to the large alkyl chains. Now the compounds are renamed **BTTBo-4F** to **DCTMR** (Figure 1). An array of chromophores (**DCTM1-DCTM6**) were formulated with push-pull architecture, and then their NLO properties were determined through density functional theory (DFT). From literature, we found that a study of the aforesaid benzotrithiophene-based compounds has not been reported yet. This research represents a step forward in the advancement of NLO matter and may represent the theoretical aspect of second-order NLO properties because of the appropriate D_1-π_1-D_2-π_2-A configuration.

RESULTS AND DISCUSSION

The study is emphasized on theoretical investigation of nonlinear optical behavior by organic nonfullerene systems. In the current study, **DCTMR** is selected as a reference after some alterations in the parent molecule (**BTTBo-4F**), which is taken from the literature as demonstrated in Figure 1.

In this study, the chain length of the π-linker is enhanced by inserting a unit of the 1*H*-pyrrol ring in each derivative (**DCTM1-DCTM6**) to comprehend the effect of π-conjugation on NLO properties. The selected reference molecule (**DCTMR**) has A−π−D−π−A conformation, but in order to achieve push−pull confirmation (D_1−π_1−D_2−π_2−A) arrangement, the terminal acceptor part, i.e., [2-(2-ethylidene-5,6-difluoro-3-oxo-indan-1-ylidene)-malononitrile], is replaced with -*N*,*N*-dimethylaniline as the donor motif to design **DCTM1** as shown in Figure 2. Further modification is done in **DCTM1** by adding the 1*H*-pyrrol unit π_2-spacer to design **DCTM2-DCTM6** derivatives. The IUPAC names of formulated molecules are given in Table S30, while their ChemDraw structures are presented in Figure S1 and data for Cartesian coordinates are tabulated in Tables S1−S7. The effect of enhanced π-conjugation on NLO properties, highest occupied molecular orbital−lowest unoccupied molecular orbital (HOMO−LUMO) band gap, optical properties, $\langle\alpha\rangle$, β_{tot}, and $\langle\gamma\rangle$ is examined. This research might be very helpful in the field of NLO and may provide a platform for experimental researchers to synthesize these compounds with improved

https://doi.org/10.1021/acsomega.3c04774
ACS Omega 2023, 8, 39288−39302

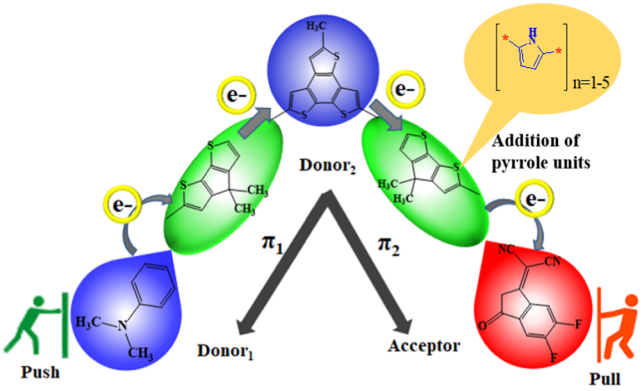

Figure 2. Sketch map of the reference and its derivative compounds (**DCTM1-DCTM6**).

NLO properties. The optimized geometries of the investigated compounds are presented in Figure S2.

Electronic Properties. The Frontier molecular orbital (FMO) analysis permits us to establish some important quantum chemistry factors, i.e., kinetic stability, electronic characteristics, electron transport ability, and chemical reactivity of an organic system.[31] The acquired energy difference ($E_{gap} = E_{LUMO} - E_{HOMO}$) of systems is proportional to the kinetic stability and helpful in the quantum chemical study of materials having NLO characteristics.[32,33] FMO investigation confirms the electronic charge distribution arrangement for the highest occupied molecular orbital (HOMO) and the lowest unoccupied molecular orbital (LUMO).[34] FMOs also play a crucial part in modeling the UV−visible spectrum and the reaction mechanism analysis of the studied compounds.[35] Therefore, DFT calculations for the current study are carried out to calculate the E_{HOMO}, E_{LUMO}, E_{HOMO-1}, E_{LUMO+1}, and ΔE of **DTCMR** and **DTCM1-DTCM6** and the outcomes are represented in Table 1.

The HOMO is illustrated to be the part having a large electron-donating tendency, such as a donor, whereas the LUMO, as well as some part of the π-spacer, is observed to be an electron-deficient region, such as an acceptor.[36] The FMO diagram (Figure 3) with blue (positive) and red (negative) sections explains the electronic cloud dispersal during ICT. A significant charge transference from HOMO toward LUMO is seen between the different parts of chromophores. In **DTCMR**, the HOMO and LUMO electronic cloud is predominantly located on the entire molecule. However, in **DTCM1-DTCM6**, the greater part of charge density in HOMO is concentrated on the π-spacers and donor, whereas for LUMO a greater amount of charge density resides on the acceptor unit. Table 2 shows that lower energy gaps in all of the designed molecules (1.600−1.802 eV) in contrast to the reference compound (2.129 eV) support their reactive

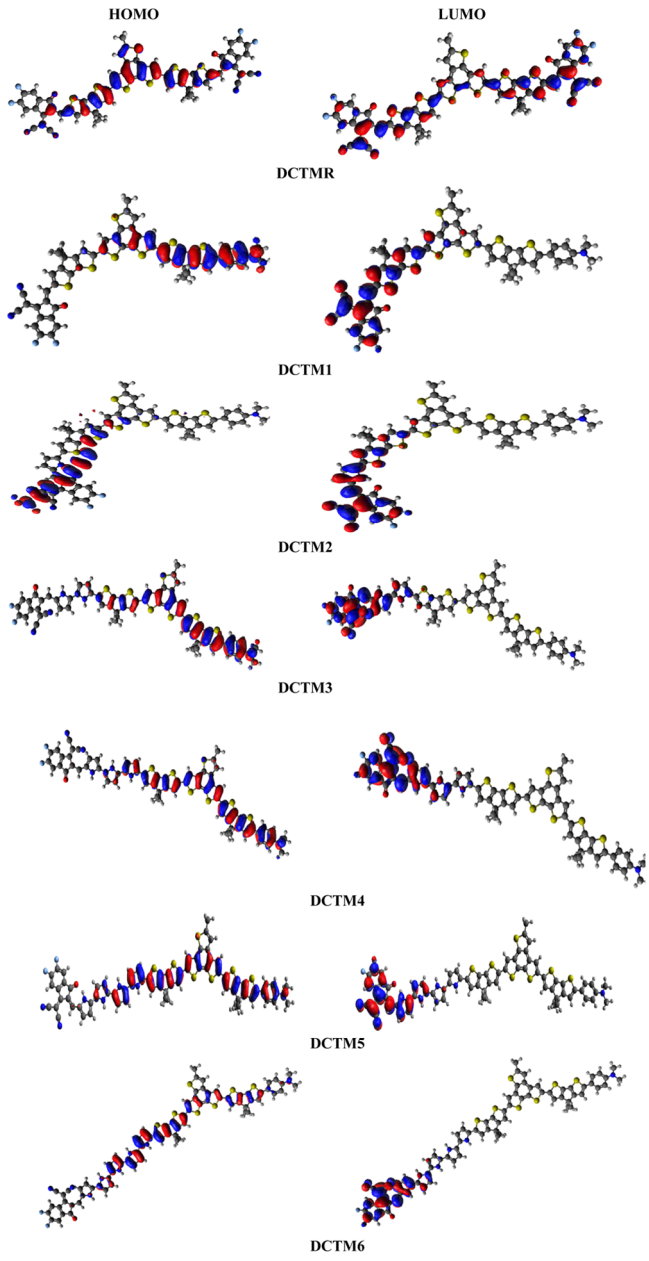

Figure 3. Counter FMOs' surfaces of **DCTMR** and **DCTM1-DCTM6**.

character with improved NLO results. The highest band gap (2.129 eV) is noted in **DTCMR** due to the A−π−D−π−A confirmation and reduced conjugation of the system. The smallest band gap (0.968 eV) (Table 1) is observed in **DTCM5** due to the addition of a π-bridge (1*H*-pyrrol), which

Table 1. Computed Energies (eV) of FMOs of DCTMR and DCTM1-DCTM6

compounds	E_{HOMO}	E_{LUMO}	ΔE	E_{HOMO-1}	E_{LUMO+1}	ΔE
DCTMR	−5.625	−3.496	2.129	−6.118	−3.361	2.757
DCTM1	−5.049	−3.368	1.681	−6.300	−1.967	4.333
DCTM2	−5.016	−3.334	1.682	−5.620	−2.108	3.512
DCTM3	−4.976	−3.174	1.802	−5.541	−2.718	2.823
DCTM4	−4.945	−3.147	1.798	−5.497	−2.263	3.234
DCTM5	−4.092	−3.124	0.968	−5.445	−2.333	3.112
DCTM6	−4.829	−3.129	1.700	−6.118	−3.361	2.757

https://doi.org/10.1021/acsomega.3c04774
ACS Omega 2023, 8, 39288−39302

Table 2. Results of UV−Vis Absorption Spectroscopy for DCTMR and DCTM1-DCTM6 in Solvent Phase and Gaseous Phase

media	compounds	λ_{max} (nm)	E_x (eV)	f_{os}	MO contributions
chloroform	**DCTMR**	726.669	1.706	3.570	H → L (94%)
	DCTM1	858.438	1.444	0.878	H → L (97%),
	DCTM2	793.854	1.562	0.731	H → L (94%), H-1 → L (5%)
	DCTM3	782.235	1.585	1.004	H-1 → L (14%), H → L (84%),
	DCTM4	792.687	1.564	1.014	H-1 → L (19%), H → L (78%),
	DCTM5	806.244	1.538	0.934	H-1 → L (14%), H → L (84%),
	DCTM6	851.715	1.456	0.729	H → L (90%), H-1 → L (8%)
gaseous phase	**DCTMR**	675.700	1.835	3.296	H → L (96%)
	DCTM1	827.610	1.498	0.694	H → L (99%),
	DCTM2	792.839	1.564	0.494	H → L (98%),
	DCTM3	787.251	1.575	0.483	H → L (97%), H-1 → L (3%)
	DCTM4	790.463	1.569	0.396	H → L (95%), H-1 → L (5%)
	DCTM5	792.130	1.565	0.387	H → L (93%), H-1 → L (7%)
	DCTM6	825.571	1.502	0.316	H → L (91%), H-1 → L (8%)

increases the conjugation of the system and facilitates the electronic charge movement from the donor to acceptor, hence making it a suitable NLO material among theoretically designed compounds. The energy gap of **DTCM1** is noted to be 2.199 times lesser than the E_{gap} of the reference compound because of the push-pull structure. The energy gap values of all compounds (**DTCM1**-**DTCM6**) lie in between 0.968−1.802 eV. The introduction of π-bridges results in enhanced conjugation, which generates the strong push−pull structure essential for a better NLO effect. The E_{gap} values of all investigated systems are in the following decreasing order: **DTCMR** (2.129 eV) > **DTCM3** (1.802 eV) > **DTCM4** (1.798 eV) > **DTCM6** (1.700 eV) > **DTCM2** (1.682 eV) > **DTCM1** (1.681 eV) > **DTCM5** (0.968 eV). Compared to other derivatives, **DCM5** exhibits a lower band gap, possibly due to favorable electronic properties or efficient charge transfer facilitated by neighboring pyrrole units. An interesting behavior was seen for the energy gap in higher orbitals. All of the fabricated molecules exhibited higher energy gap (E_{gap}) values than the reference molecule. This unique behavior of compounds might open new ways for researchers. Overall, an efficient charge transmission is noticed in the formulated molecules in contrast to **DTCMR**, which is a measure of their polarizable character and the reactivity of NLO materials.

Density-of-States Investigation. To support the FMOs outcomes, a density-of-states (DOS) investigation is performed. For this purpose, the studied molecules are distributed into three segments, i.e., donor, π-spacer, and acceptor parts, and characterized by red-, green-, and blue-colored lines, respectively, as shown in Figure S3. The band gap is a key feature of the band structure, which has the power to significantly change the electronic and optical characteristics of the compounds.[37] Figure S3 shows that in the reference molecules (DCTMR), the electronic cloud of HOMOs is equally distributed over the donor (D_1), while in the case of LUMOs, the charge concentration majorly resides over the acceptor segment (Figure 3). The FMO study shows that HOMOs mainly reside over donor and π-spacer regions, whereas in the case of LUMOs, the electronic cloud majorly lies over the acceptor moiety. The DOS study reveals that donors (D_1 and D_2) contribute 40.1, 49.3, 48.1, 45.0, 27.8, 27.3, and 16.4% to HOMO and 9.4, 7.4, 2.8, 0.6, 0.2, 0.0, and 0.0% to LUMO for DCTMR and DCTM1-DCTM6, respectively. In a similar fashion, the π-spacer (π_1 and π_2) contributes 43.3, 49.5, 50.2, 50.7, 60.2, 43.0, and 33.4% to HOMO, while on LUMO its participation is 36.7, 35.2, 15.8, 3.7, 0.9, 0.3, and 0.1% for DCTMR and DCTM1-DCTM6, respectively. Moreover, the charge contribution of the acceptor at HOMO is 16.6, 1.2, 1.7, 4.3, 12.0, 29.7, and 50.1%; however, it contributes 53.9, 57.4, 81.4, 95.7, 98.9, 99.7, and 99.9% to LUMO for DCTMR and DCTM1-DCTM6, respectively. Furthermore, the DOS graph shows that HOMOs' highest electronic cloud is located on donors D_1 and D_2, as a red high peak is found at almost −6.3 eV, whereas the electron charge concentration is traced to be near 1.5 eV on the acceptor group for LUMOs. This efficient charge transference in a chromophore elucidates that these fabricated organic systems might possess effective NLO properties.

Optical Properties. The ultraviolet−visible (UV−vis) spectral study determines the various linear optical parameters as well as nonlinear optical activity of the formulated compounds.[3] The UV−vis investigation is accomplished to study the charge transfer possibility, maximum absorption (λ_{max}), and electronic excitation energy (E_x) besides oscillation frequency (f_{os}) of the investigated molecules. All of these parameters are computed in the gaseous along with solvent phase (chloroform), as shown in Table 2. The six lowest singlet−singlet transitions are shown in Tables S8−S21.

It is clear from the outcomes (Table 2) that the maximum absorption that occurs in chloroform is approximated to the experimental outcome of 705 nm reported in the reference molecule (**DCTMR**).[30] Among all of the designed compounds, the absorption maxima is observed in **DCTM1** at 858.438 nm with an excitation energy (E_x) of 1.444 eV, analogous to the molecular orbital transition H → L (97%) and oscillator strength of 0.878; therefore, these transitions would be strongly allowed. Hence, it is regarded as a red-shifted compound, which might be attributed to its distinctive chemical design. The wavelength (nm) trend in the gaseous phase in the investigated compounds is **DCTM1** (858.438 nm) > **DCTM6** (851.715 nm) > **DCTM2** (793.854 nm) > **DCTM4** (792.687 nm) > **DCTM5** (806.244 nm) > **DCTM3** (782.235 nm) > **DCTMR** (726.669 nm). However, their relative transition energies are observed to be in the reverse order, as **DCTM2** (1.444 eV) < **DCTMR** (1.456 eV) < **DCTM6** (1.538 eV) < **DCTM5** (1.562 eV) < **DCTM4** (1.564 eV) < **DCTM3** (1.585 eV) < **DCTM1** (1.706 eV). Meanwhile, the oscillator strength is seen to be in the following order: **DCTMR** (3.570) > **DCTM1** (1.014) > **DCTM4** (1.004) > **DCTM2** (0.878) > **DCTM5** (0.934) > **DCTM3** (0.731) > **DCTM6** (0.729).

In the gaseous phase, **DCTMR** showed the maximum wavelength = 675.700 nm, with the transition energy and oscillation frequency as 1.835 eV and 3.296, respectively, and the major HOMO → LUMO contributions were observed to be 96%. However, all of the derivatives exhibit λ_{max} in the range of 787.251−827.610 nm and oscillator strength in the range of 0.316−0.694. Moreover, among all of the derivative compounds, **DCTM3** shows a blue shift (787.251 nm) as the

https://doi.org/10.1021/acsomega.3c04774
ACS Omega 2023, 8, 39288−39302

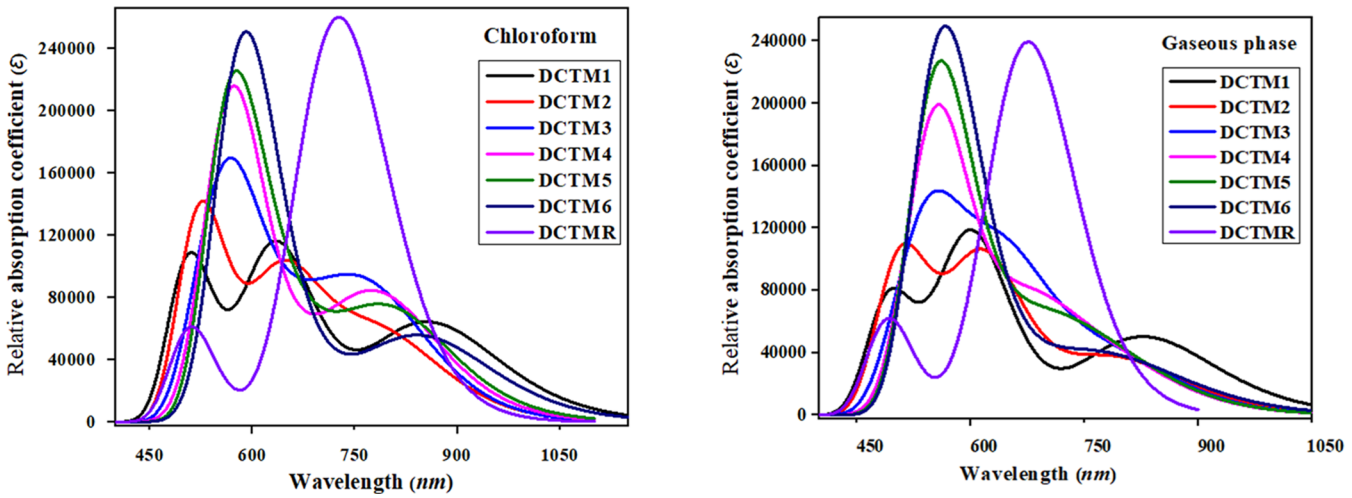

Figure 4. Simulated absorption spectra of **DCTMR** and **DCTM1-DCTM6** in chloroform and the gaseous phase.

Table 3. Global Reactivity Parameters (in eV) for DCTMR and DCTM1-DCTM6

compounds	IP	EA	X	η	μ	ω	σ	ΔN_{max}
DCTMR	5.625	3.496	4.561	1.065	−4.561	9.769	0.470	2.922
DCTM1	5.049	3.368	4.209	0.841	−4.209	10.536	0.595	5.005
DCTM2	5.016	3.224	4.120	0.896	−4.120	9.472	0.558	4.598
DCTM3	4.979	3.174	4.077	0.903	−4.077	9.207	0.554	3.174
DCTM4	4.945	3.147	4.046	0.899	−4.046	9.105	0.556	4.501
DCTM5	4.902	3.124	4.013	0.889	−4.013	9.057	0.562	4.514
DCTM6	4.829	3.129	3.979	0.850	−3.979	9.313	0.588	4.681

maximum wavelength and a higher energy 1.575 eV with the oscillation transition as 0.483 (Table 2). Further, **DCTM1** shows λ_{max} at 827.610 nm, transition energy 1.498 eV, oscillator transition energy 0.649, and major H-1 → L molecular orbital contributions = 99%. Overall, the λ_{max} of all of the above-mentioned compounds in gaseous phase is observed to be **DCTM1** (827.610 nm) > **DCTM6** (825.571 nm) > **DCTM2** (792.839 nm) > **DCTM5** (792.130 nm) > **DCTM4** (790.463 nm) > **DCTM3** (787.251 nm) > **DCTMR** (675.700 nm). The efficiency of NLO materials can also be determined by the excitation energy, i.e, a lower excitation energy provides a higher power conversion efficiency (PCE). The UV−vis absorption spectra in both solvent (chloroform) and gaseous phases are displayed in Figure 4.

Global Reactivity Parameters (GRPs). The GRPs are estimated via HOMO−LUMO energy values[38] to predict the chemical nature of the molecules. A higher E_{HOMO} value indicates a stronger electron donation tendency, whereas a lower value of E_{LUMO} indicates a better ability to accept electrons.[39,40] According to Pearson, the molecules with a lower value of energy band gap ($E_{LUMO} - E_{HOMO}$) are soft and highly reactive in nature.[41] The softness of a molecule is correlated to its hardness and articulates the extent of chemical reactivity.[42] The electronegativity (X),[43] ionization potential (IP),[44] electron affinity (EA),[45] global softness (σ),[46] hardness (η),[47] chemical potential (μ),[48] and electrophilicity index (ω)[49] are the GRPs, which are described using the HOMO−LUMO energy band gap[50,51] and the outcomes are listed in Table 3.

Electronic affinity (EA) is the tendency to accept an electron from the donor; therefore, it is calculated by the energy of LUMO using eq 1.

$$\mathrm{EA} = -E_{\mathrm{LUMO}} \tag{1}$$

The ionization potential is entrenched using HOMO and by applying eq 2.

$$\mathrm{IP} = -E_{\mathrm{HOMO}} \tag{2}$$

A molecule's resistance to intramolecular charge transfer (ICT) is measured by its chemical hardness; the lower the chemical hardness, the higher the ICT.[41] Mulliken found a relationship between the electronegativity and the mean of HOMO−LUMO energies.[52] Therefore, in order to calculate the hardness, softness, and electronegativity, eqs 3−5[53] are employed.

$$\eta = \frac{[\mathrm{IP} - \mathrm{EA}]}{2} \tag{3}$$

$$\sigma = \frac{1}{2\eta} \tag{4}$$

$$X = \frac{[\mathrm{IP} + \mathrm{EA}]}{2} \tag{5}$$

The μ and ω are calculated using eq 6[51] and 7,[54,55] respectively.

$$\mu = \frac{E_{\mathrm{HOMO}} + E_{\mathrm{LUMO}}}{2} \tag{6}$$

$$\omega = \frac{\mu^2}{2\eta} \tag{7}$$

The ability of a compound to absorb more electrical charge from its environment is denoted by ΔN_{max}, and is calculated by eq 8[51]

https://doi.org/10.1021/acsomega.3c04774
ACS Omega 2023, 8, 39288−39302

Table 4. Selected Values of Natural Bond Orbitals Analysis for the Reference (DCTMR) and Derivative (DCTM1-DCTM6) Molecules

compounds	donor (i)	type	acceptor (j)	type	$E(J)E(i)^b$	$F(i,j)^c$	$E(J)E(i)^b$
DCTMR	C35−C36	π	C65−C66	π^*	33.76	0.31	0.091
	C97−N98	π	C99−N100	π^*	0.88	0.47	0.018
	C65−H67	σ	C35−S39	σ^*	10.72	0.73	0.079
	C97−N98	σ	C88−C92	σ^*	0.50	1.68	0.026
	S45	LP(2)	C41−C42	π^*	30.19	0.27	0.081
	O101	LP(2)	C72−C89	σ^*	21.32	0.75	0.115
DCTM1	C72−C73	π	C74−S75	π^*	37.94	0.17	0.086
	C57−O59	π	C54−C56	π^*	3.96	0.43	0.04
	C54−H55	σ	C74−S75	σ^*	10.78	0.73	0.079
	C101−N102	σ	C93−C100	σ^*	0.50	1.68	0.026
	N60	LP(1)	C47−C51	π^*	50.23	0.28	0.111
	O59	LP(2)	C57−C92	σ^*	21.33	0.75	0.114
DCTM2	C61−C63	π	C100−C107	π^*	29.55	0.29	0.083
	C108−N109	π	C110−N111	π^*	0.90	0.47	0.018
	C61−H62	σ	C57−N58	σ^*	9.52	0.99	0.087
	C108−N109	σ	C100−C107	σ^*	0.50	1.67	0.026
	N67	LP(1)	C47−C51	π^*	49.90	0.28	0.111
	O66	LP(2)	C64−C99	σ^*	20.49	0.78	0.115
DCTM3	C99−C100	π	C54−C55	π^*	28.92	0.30	0.084
	C98−N111	π	C117−N118	π^*	0.71	0.47	0.016
	C54−H120	$\sum$	C55−C56	σ^*	8.98	1.05	0.087
	C115−N116	$\sum$	C56−C113	σ^*	0.51	1.66	0.026
	N58	LP(1)	C47−C51	π^*	49.45	0.29	0.111
	O114	LP(2)	C57−C70	σ^*	21.14	0.74	0.113
DCTM4	C118−C119	π	C120−C121	π^*	30.9	0.29	0.086
	C81−N82	π	C79−N80	π^*	0.71	0.48	0.016
	C54−H83	$\sum$	C55−C71	σ^*	8.91	1.05	0.086
	C79−N80	$\sum$	C71−C78	σ^*	0.51	1.66	0.026
	N122	LP(1)	C118−C119	π^*	50.31	0.30	0.110
	O58	LP(2)	C56−C70	σ^*	21.14	0.74	0.113
DCTM5	C113−C114	π	C115−N116	π^*	35.43	0.22	0.092
	C135−N136	π	C133−N134	π^*	0.90	0.47	0.018
	C54−H77	σ	C121−N126	σ^*	9.56	0.99	0.087
	C135−N136	σ	C56−C131	σ^*	0.50	1.67	0.026
	N58	LP(1)	C47−C51	π^*	49.64	0.28	0.111
	O132	LP(2)	C57−C70	σ^*	20.54	0.77	0.114
DCTM6	C131−C132	π	C133−C134	π^*	31.13	0.29	0.086
	C71−C78	π	C79−N80	π^*	0.94	0.41	0.019
	C54−H83	σ	C55−C71	σ^*	8.90	1.05	0.086
	C79−N80	σ	C71−C78	σ^*	0.51	1.66	0.026
	N135	LP(1)	C131−C132	π^*	50.37	0.30	0.110
	O58	LP(2)	C56−C70	σ^*	21.14	0.74	0.113

$$\Delta N_{max} = -\mu/\eta \quad (8)$$

The outcomes of Table 3 disclose that all of the compounds under study possess a high ionization potential with a low value of electron affinity. However, among all of the examined compounds, the reference (**DCTMR**) exposed the highest IP with a value of 5.625 eV. The ionization potential is observed to be decreasing in the following order: **DCTMR** > **DCTM1** > **DCTM2** > **DCTM3** > **DCTM4** > **DCTM5** > **DCTM6**. Further, **DCTM1** exhibits a higher softness value of 0.595 eV^{-1} with the lowest band gap (1.600 eV) among the rest of the molecules; therefore, it is the most reactive and polarizable compound.[56] The lower the value of chemical hardness, the less stable is the molecule.[57] The highest value of hardness (1.065 eV) is shown by **DCTMR**. All of the designed compounds are arranged in decreasing order on the basis of softness as **DCTM1** > **DCTM6** > **DCTM5** > **DCTM2** > **DCTM4** > **DCTM3** > **DCTMR**. Moreover, 4.561 and 3.979 eV are the highest and lowest values of electronegativity demonstrated by **DCTMR** and **DCTM6**, respectively. Additionally, the highest ΔN_{max} is exposed by **DCTM1** with a value of 5.005 eV. The computed values of ΔN_{max} are observed to be decreased in the following order: **DCTM1** > **DCTM6** > **DCTM2** > **DCTM5** > **DCTM4** > **DCTM3** > **DCTMR**. In conclusion, all of the results of GRPs show that **DCTM1** has the highest charge transfer (CT) and lowest band gap (Table 1); hence, it displays the maximum ICT and will prove as the best optoelectronic material for future NLO applications.

Natural Bond Orbital (NBO) Study. The natural bond orbital (NBO) study is usually performed to examine the molecular stability emerging due to the charge delocalization and hyper-conjugative interactions.[58] The substantial ICT interactions from the donor to the acceptor and the energy

https://doi.org/10.1021/acsomega.3c04774
ACS Omega 2023, 8, 39288−39302

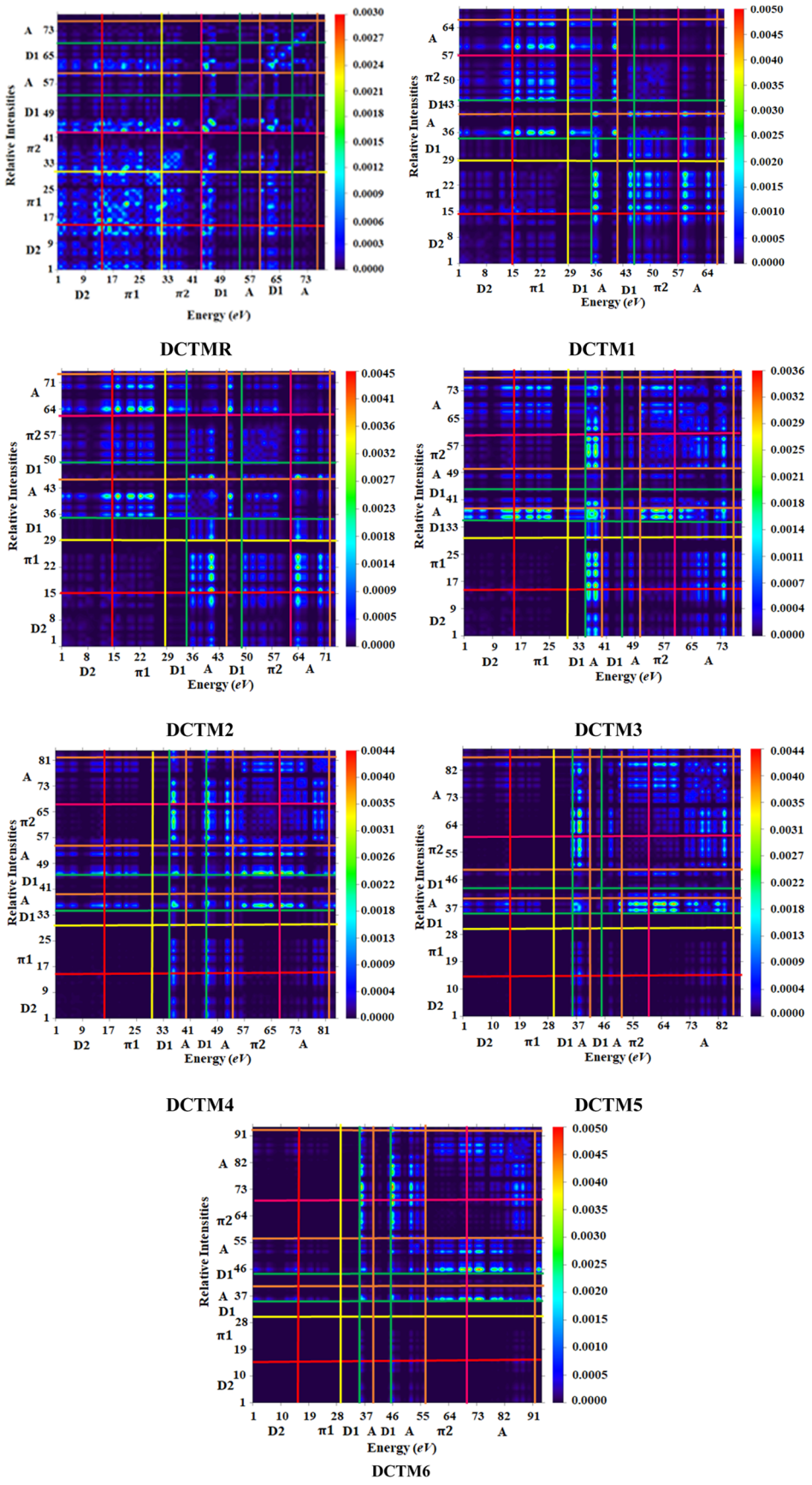

Figure 5. Transition density matrix pictographs of DCTMR and DCTM1 to DCTM6.

https://doi.org/10.1021/acsomega.3c04774
ACS Omega 2023, 8, 39288−39302

contribution to these interactions to stabilize the system are given by the second-order perturbation theory study of the Fock matrix in NBO basis, and the outcomes are recorded in Tables S22−S28 (Supporting Information). The NBO examination for **DCTMR** and its derivative compounds (**DCTM1-DCTM6**) was accomplished at MPW1PW91/6-311G(d,p) level of theory and the selected transitions are recorded in Table 4. Equation 9 is used to compute the energy of stabilization $E^{(2)}$ in the NBO investigation.[59]

$$E^{(2)} = q_i \frac{(F_{i,j})^2}{\varepsilon_j - \varepsilon_i} \tag{9}$$

where the donor and acceptor segments are represented by I and j subscripts, $E^{(2)}$ is the energy of stabilization, and q_i, ε_i, ε_j, and $F_{i,j}$ characterize the orbital occupancy, diagonal, and off-diagonal NBO Fock matrix components, respectively.[60]

The natural bond orbital analysis shows that four main transition types ($\sigma \rightarrow \sigma^*$, $\pi \rightarrow \pi^*$, LP $\rightarrow \sigma^*$, and LP $\rightarrow \pi^*$) are observed for the reference (**DTCMR**) and its derivatives (**DCTM1-DCTM6**). Among these, $\pi \rightarrow \pi^*$ transitions are essential for ICT and stabilization of the compound. The transitions π(C35−C36) → π^*(C65−C66), π(C72−C73) → π^*(C74−S75), π(C61−C63) → π^*(C100−C107), π(C99−C100) → π^*(C54−C55), π(C118−C119) → π^*(C120−C121), π(C113−C114) → π^*(C115−N116), and π(C131−C132) → π^*(C133−C134) provide the highest stabilization energy values of 33.76, 37.94, 29.55, 28.92, 30.9035.43, and 31.33 kcal·mol^{-1}, respectively, for **DCTMR** and **DCTM1-DCTM6**, while π(C97−N98) → π^*(C99−N100), π(C57−O59) → π^*(C54−C56), π(C108−N109) → π^*(C110−N111), π(C98−N111) → π^*(C117−N118), π(C81−N82) → π^*(C79−N80), π(C135−N136) → π^*(C133−N134), and π(C71−C78) → π^*(C79−N80) transitions have the lowest stabilization energies such as 0.88, 3.96, 0.90, 0.71, 0.71, 0.90, and 0.94 kcal·mol^{-1}, respectively, for reference and designed molecules.

Moreover, $\sigma \rightarrow \sigma^*$ transitions such as σ(C65−H67) → σ^*(C35−S39), σ(C54−H55) → σ^*(C74−S75), σ(C61−H62) → σ^*(C57−N58), σ(C54−H120) → σ^*(C55−C56), σ(C54−H83) → σ^*(C55−C71), σ(C54−H77) → σ^*(C121−N126), and σ(C54−H83) → σ^*(C55−C71) have 10.72, 10.78, 9.52, 8.98, 8.91, 9.56, and 8.90 kcal·mol^{-1} as the highest energies for **DCTMR** and **DCTM1-DCTM6**, respectively. Similarly, σ(C97−N98) → σ^*(C88−C92), σ(C101−N102) → σ^*(C93−C100), σ(C108−N109) → σ^*(C100−C107), σ(C115−N116) → σ^*(C56−C113), σ(C79−N80) → σ^*(C71−C78), σ(C135−N136) → σ^*(C56−C131), and σ(C79−N80) → σ^*(C71−C78) have 0.50, 0.50, 0.50, 0.51, 0.51, 0.50, and 0.51 kcal·mol^{-1}, respectively, for **DCTMR** and **DCTM1-DCTM6**. Furthermore, in the reference (**DCTMR**) and designed molecules (**DCTM1-DCTM6**), the transitions LP2(S45) → π^*(C41−C42), LP1(N60) → π^*(C47−C51), LP1(N67) → π^*(C47−C51), LP1(N58) → π^*(C47−C51), LP1(N122) → π^*(C118−C119), LP1(N58) → π^*(C47−C51), and LP1(N135) → π^*(C131−C132) have the highest energy values as 30.19, 50.23, 49.90, 49.45, 50.31, 49.64, and 50.37 kcal·mol^{-1}, respectively, whereas the highest energy values of 21.32, 21.33, 20.49, 21.14, 21.14, 20.54, and 21.14 kcal·mol^{-1} are observed for LP2(O101) → σ^*(C72−C89), LP2(O59) → σ^*(C57−C92), LP2(O66) → σ^*(C64−C99), LP2(O114) → σ^*(C57−C70), LP2(O58) → σ^*(C56−C70), LP2(O132) → σ^*(C57−C70), and LP2(O58) → σ^*(C56−C70), respectively.

The above-mentioned results exposed that across all of the studied compounds, **DCTM1** possesses enhanced stability due to the prolonged π-conjugation between the bonding and antibonding orbitals of the thiophene ring C72−C73 bond and the C74−S75 bond stabilizes the molecule with an energy of 37.94 kcal·mol^{-1}(Table 4). Hence, NBO analysis of the aforesaid molecules shows that strong intramolecular charge transfer and prolonged hyperconjugation play a significant role in the stabilization of these compounds and endow them with tremendous NLO properties.

Hole−Electron Interaction Analysis. Multiwfn 3.8 is a powerful tool used to perform electron excitation analysis. It also offers a thorough understanding of all kinds of electron transference character. It is a highly useful method to determine the type and nature of electron excitation.[8,61] The designed compounds have *N*,*N*-dimethylaniline and 2,5,8-trimethylbenzo[1,2-*b*:3,4′:6,5-*b*]trithiophene as the donor, linked with 4,4-dimethyl-4*H*-cyclopenta[1,2-*b*:5,4-*b*′]-dithiophene as the π-linker, and at the other terminal, [2-(2-ethylidene-5,6-difluoro-3-oxo-indan-1-ylidene)-malononitrile] as a strong electron-withdrawing group. Hence, it is decided to perform a hole−electron interaction analysis in order to investigate the electron excitation behavior of our designed molecules. First, the compounds are optimized by the MPW1PW91/6-311G(d,p) method, and the six lowest singlet states are investigated. It can be seen from the hole−electron map (Figure S4) that the hole and electron of S0 → S2, S3 and S4 are scattered in the local region. Further, it is also observed that in the reference molecule (**DCTMR**), the hole is produced in a carbon atom present in the thiophene ring (π-spacer); however, electron density showed concentrated carbon atoms of the π-linker at the opposite terminal. Figure S4 also reveals that the hole intensity is intense at several parts of the π-linker and donor (D_1 and D_2), while the electron density is transferred toward the acceptor group. In **DCTM3** and **DCTM4**, a high hole intensity is observed over the carbon atom of the donor group, while the electron intensity is found to be maximum over the acceptor region. In short, all of the designed compounds, including the reference molecule, seem to be electron-type owing to the intense electron density at the electronic band, contrary to the hole band-holding hole intensity.

Transition Density Matrix (TDM) Inspection. TDM analysis was done to comprehend the ICT pattern and types of transition in the excited state.[62] For any transition between two eigen states in a many-body system, the TDM analysis provides a distinctive spatial heat map that depicts the scattering of related electron−hole pairs and enables measurement of their delocalization and coherence durations.[63,64] The electronic charge transfer from the donor (D) toward acceptor (A) moieties with the aid of a π-linker in the excited state using three-dimensional graphs is efficiently explained through this investigation.[65] In TDM analysis, hydrogen (H) atoms have been automatically neglected due to their minor involvement in the transitions. For TDM inspection, we have split DCTMR into three segments, namely terminal acceptor (A), π-bridge, and donor; however, the derivatives (DCTM1-DCTM6) are derived into five parts: donor 1 (D_1), π-spacer 1, donor 2 (D_2), π-spacer 2, and terminal acceptor (A) unit.

Figure 5 shows that all of the investigated systems show a similar behavior, in which the electronic charge density has

https://doi.org/10.1021/acsomega.3c04774
ACS Omega 2023, 8, 39288−39302

efficiently been transported diagonally out of the donor to the acceptor through the π-spacer, which permits proficient charge transmission without any hindrance. Overall, the outcomes of TDM heat maps elaborate efficient charge separation from the ground state to the excited state (S0 → S1). Interestingly, for all of the derivatives, a snapshot of **DCTM5** reveals that an efficient diagonal charge transmission coherence is only seen at the acceptor section, which supports the FMO findings. However, estimates of TDM snapshots of **DCTM1-DCMT6** suggested that exciton separation in the excited state is schematic, simpler, and developed, which might be useful in future applications.

Exciton Binding Energy (E_b). The binding energy (E_b) is another significant tool for predicting the optoelectronic properties of various materials. A stronger NLO response is produced by the increased charge mobilities caused by a low binding energy. The exciton binding energies of DCTMR and DCTM1-DCTM6 can be calculated by subtracting the first excitation energies (E_{opt}) from the band gap value (E_{gap}) with the help of eq 10.[66] The theoretically calculated values of exciton binding energies (E_b) for the investigated compounds are listed in Table 5.

$$E_b = E_{LH} - E_{opt} \quad (10)$$

Table 5. E_{LH}, E_{opt}, and E_b of the Investigated Compounds (DCTMR and DCTM1-DCTM6) in eV[a]

compounds	$E_{L\text{-}H}$	E_{opt}	E_b
DCTMR	2.129	1.706	0.423
DCTM1	1.600	1.946	−0.346
DCTM2	1.682	1.907	−0.225
DCTM3	1.802	2.136	−0.336
DCTM4	1.798	2.127	−0.329
DCTM5	1.778	2.141	−0.363
DCTM6	1.700	2.145	−0.445

[a] $E_{LH} = E_{LUMO} - E_{HOMO}$, E_{opt} = first singlet excitation energies and E_b = exciton binding energy.

Here, E_L and E_H are the energies of LUMOs and HOMOs, respectively. The formulated systems illustrate a high charge dissociation capability, giving a low value of E_b. The value of E_b reduces in the following order: **DCTMR** (0.423 eV) > **DCTM2** (−0.225 eV) > **DCTM4** (−0.329 eV) > **DCTM3** (−0.336 eV) > **DCTM1** (−0.346 eV) > **DCTM5** (−0.363 eV) > **DCTM6** (−0.445 eV). Among all of the titled chromophores, **DCTM6** demonstrated the lowest value (−0.445 eV) of binding energy, exposing its high optoelectronic characteristics with a greater magnitude of exciton dissociation in the excited state (S_1). In a nutshell, all of the examined molecules have E_b values less than 1.9 eV and are found suitable for optical activity and a range of nonlinear optical applications.

Molecular Electrostatic Potential (MEP). Molecular electrostatic potential (MEP) surface analysis plays an important role in the understanding of effective NLO materials.[67] The MEP pictographs for reference and derivatives are displayed in Figure 6. The negative and positive charge densities are shown by red- and blue-colored regions, respectively, which are suitable for electrophilic as well as nucleophilic attack. The declining order of electronic charge participation and electrostatic potential is as blue > green > yellow > orange > red.[81]

The red portion represents the highly electronegative (EN) fluorene (F) and oxygen (O) atoms and is prone to nucleophilic attack, while green and yellow colors present chlorine (Cl) and sulfur (S) atoms, respectively, which are less EN, demonstrating the easier electrophilic attack at these particular points, because of the thick electronic charge density of F, O, Cl, and S atoms. Moreover, blue color indicates the nitrogen (N) atom with negative potential, while gray color represents the electropositive carbon (C) and hydrogen (H) atoms, presenting promising positions for nucleophilic attack. From the above-mentioned results, it can be concluded that electrophilic species are the best to attack the yellow- and red-colored regions over molecular electrostatic potential (MEP) surface, whereas nucleophilic species are observed as the best to attack the blue regions over the MEP surface.[68]

Nonlinear Optical (NLO) Study. The NLO study has been acknowledged as the most suitable study for the progress of various areas such as photonic materials,[69] optical devices,[70] photonic devices,[71] electrochemical sensors, optoelectronics, biomedicine,[72] and high-speed optical signal processing.[73] For developing the NLO response, a pull−push configuration of

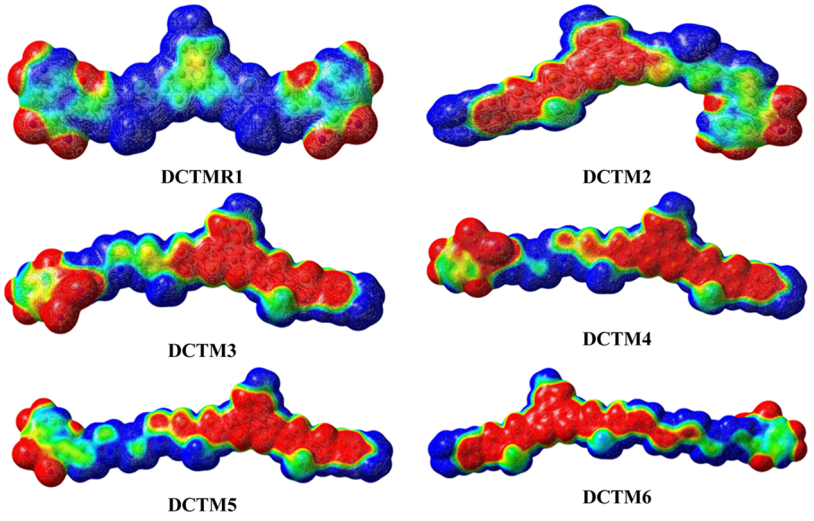

Figure 6. Molecular electrostatic potential surfaces of reference and designed compounds.

https://doi.org/10.1021/acsomega.3c04774
ACS Omega 2023, 8, 39288−39302

compounds is created, whose robustness depends upon the type of donor and acceptor moieties that are interconnected via the π-network.[18] The NLO property is correlated to the calculated values elucidating the structural characteristics, electronic response, linear polarizability ($\langle\alpha\rangle$), first hyperpolarizability (β_{tot}), and second hyperpolarizability (γ_{tot}), which explain the band gap and molecular structure.[40,74] Hence, to estimate how donor and acceptor moieties affected the linear and nonlinear behaviors of **DTCMR** and **DTCM1-DTCM6**, their $\langle\alpha\rangle$, β_{tot}, and γ_{tot} were computed and their simulated values are displayed in Tables 6–9. The average polarizability $\langle\alpha\rangle$[75] value is determined using eq 11.

Table 6. Total Dipole Moments (μ) and Their Major Contributing Tensors[a]

compounds	μ_x	μ_y	μ_z	μ_{tot}
DCTMR	−0.495	−5.545	−0.018	5.567
DCTM1	−19.688	3.582	−0.215	20.012
DCTM2	16.226	8.316	−0.839	18.252
DCTM3	15.580	1.766	−4.393	16.284
DCTM4	−16.998	−7.502	3.090	18.835
DCTM5	−19.958	2.355	−1.243	20.135
DCTM6	−16.110	8.044	−4.717	18.614

[a]Units in Debye (D).

$$\langle a\rangle = 1/3(\alpha_{xx} + \alpha_{yy} + \alpha_{zz}) \quad (11)$$

(β_{tot})[76] and (γ_{tot})[77] are estimated with the help of eqs 12 and 13.

$$\beta_{tot} = (\beta_x^2 + \beta_y^2 + \beta_z^2)^{1/2} \quad (12)$$

where $\beta_x = \beta_{xxx} + \beta_{xyy} + \beta_{xzz}$, $\beta_y = \beta_{yyy} + \beta_{xxy} + \beta_{yzz}$, $\beta_z = \beta_{zzz} + \beta_{xxz} + \beta_{yyz}$

$$\gamma_{tot} = \sqrt{\gamma_x^2 + \gamma_y^2 + \gamma_z^2} \quad (13)$$

where $\gamma_i = \frac{1}{15}\sum_j (\gamma_{ijji} + \gamma_{ijij} + \gamma_{iijj})$ $i, j = \{x, y, z\}$

The dipole moment is calculated by utilizing eq 14.

$$\mu = (\mu_x^2 + \mu_y^2 + \mu_z^2)^{1/2} \quad (14)$$

The product of charge magnitudes and the distance between them is called dipole moment (μ) and it is an essential feature to determine the polarizability of organic compounds.[78] Table 6 indicates the total calculated values of dipole moment (μ_{tot}) along with the 3D tensors along the *x*-, *y*-, and *z*-axis.

All of the derivatives (**DTCM1-DTCM6**) demonstrated a higher dipole moment (16.28−20.13 D) than that of the reference compound (5.567 D). Among all of the investigated compounds, the highest μ_{tot} value is observed for **DTCM5** (20.13 D) due to the presence of five 1*H*-pyrrol polymeric units that are a part of π_2. The literature survey disclosed that *para*-nitroaniline (*p*-NA) is used as a standard molecule for comparative analysis in NLO study and the dipole moment for *p*-NA is reported as 6.3 *D*.[79] The μ_{tot} values of **DTCMR** and **DTCM1-DTCM6** are 0.883, 3.176, 2.897, 2.584, 2.989, 3.195, and 2.954 times greater than those of *p*-NA, respectively. The greater values of μ_{tot} for the designed compounds create greater polarizability in them. In all of the investigated molecules, the higher μ_{tot} values are observed along μ_x (**DTCM1** = −19.688, **DTCM2** = 16.226, **DTCM3** = 15.580, **DTCM4** = −16.998, **DTCM5** = −19.958 and **DTCM6** = −16.110 D) except for **DTCMR**, which showed a greater value along μ_y (−5.545 D), respectively.

Furthermore, linear polarizability of the investigated compounds was also studied and all of the designed molecules showed comparable values of $\langle\alpha\rangle$ with **DTCMR**.

The results in Table 7 show that all of the entitled compounds demonstrated higher $\langle\alpha\rangle$ responses along the *x*-axis (α_{xx}), indicating that polarization occurred along the *x*-axis. Overall, the $\langle\alpha\rangle$ values of the entitled molecules decrease in the following order: **DTCM6** (3.456×10^{-22}) > **DTCM5** (3.308×10^{-22}) > **DTCMR** (3.162×10^{-22}) > **DTCM4** (3.116×10^{-22}) > **DTCM3** (2.958×10^{-22}) > **DTCM2** (2.739×10^{-22}), and **DTCM1** (2.715×10^{-22} esu).

Table 7. Major Contributing Tensors ($\times 10^{-22}$ esu) of Linear Polarizabilities

compounds	α_{xx}	α_{yy}	α_{zz}	$\langle\alpha\rangle$ ($\times 10^{-22}$ esu)
DCTMR	6.733	2.099	0.653	3.162
DCTM1	5.178	2.283	0.683	2.715
DCTM2	4.589	2.918	0.710	2.739
DCTM3	5.882	2.152	0.841	2.958
DCTM4	6.372	2.098	0.877	3.116
DCTM5	6.765	2.246	0.912	3.308
DCTM6	6.988	2.308	0.107	3.456

The improvement in hyperpolarizability values in **DTCM1-DTCM6** is associated with the delocalization of π-electrons arising from the addition of π-bridges in the molecules. This delocalization lowers the LUMO−HOMO band gap. As it is revealed by the literature, the polarizability of compounds is highly influenced by the LUMO/HOMO band gap; the lower the band gap, the higher the polarizability amplitudes, and vice versa. The β_{tot} and its contributing tensor values are calculated for the said functional and basis sets, and the results are recorded in Table 8.

The β_{tot} value of **DTCMR** is 0.8840×10^{-27} esu and all designed derivatives indicated notable results ($3.9060-7.0440 \times 10^{-27}$ esu) than that of **DTCMR** due to the strong push−pull architecture. Moreover, a systematic connection is noticed between the β_{tot} values and the molecular structures. The β_{tot} usually increases with the extended conjugation, which is achieved by the introduction of π-spacers in the system, which promotes the nonlinearity in the molecule. On the basis of the above-mentioned results, the highest β_{tot} is examined for **DTCM1**, i.e., 7.0440×10^{-27} esu. The reason for this enhancement might be the addition of the π-spacer unit (1*H*-pyrrol) in the structure of **DTCM1**. Overall, the descending order of β_{tot} values of all of the mentioned molecules is as follows: **DTCM1** (7.0440×10^{-27}) > **DTCM6** (4.1040×10^{-27}) > **DTCM3** (4.0880×10^{-27}) > **DTCM5** (4.0090×10^{-27}) > **DTCM2** (3.9780×10^{-27}) > **DTCM4** (3.9060×10^{-27}) > **DTCMR** (0.8840×10^{-27} esu). Among the major contributing tensor components, β_{xxx} unveils highest values, which produce a better ICT along the *x*-axis. A comparative study is also carried out using *p*-NA as a standard molecule ($\beta_{tot} = 9.6 \times 10^{-30}$ esu).[79] The β_{tot} values calculated for **DTCMR** and **DTCM1-DTCM6** are 92.08, 757.42, 427.74, 439.57, 420.00, 431.08, and 431.61 times greater than that of the standard molecule, respectively. This comparative analysis

https://doi.org/10.1021/acsomega.3c04774
ACS Omega 2023, 8, 39288−39302

Table 8. Calculated First Hyperpolarizability (β_{tot}) along its Major Contributing Tensors (esu) of the Investigated Molecules

systems	DCTMR × 10^{-27}	DCTM1 × 10^{-27}	DCTM2 × 10^{-27}	DCTM3 × 10^{-27}	DCTM4 × 10^{-27}	DCTM5 × 10^{-27}	DCTM6 × 10^{-27}
β_{xxx}	0.0227	−6.6990	3.270	3.800	−3.769	−3.883	−3.722
β_{xxy}	0.8636	0.3908	0.5124	0.4327	0.0236	−0.1916	0.0195
β_{xyy}	0.01155	−0.3369	0.6388	0.2524	−0.0811	−0.5261	−0.0912
β_{yyy}	0.0193	0.0094	0.2272	0.0407	−0.0011	0.0016	0.0093
β_{xxz}	0.0013	0.0020	−0.0010	−0.1543	0.3822	−0.4843	−0.9482
β_{yyz}	0.0008	0.0047	−0.0010	−0.0176	0.0019	−0.0048	−0.0039
β_{xzz}	−0.0002	0.0039	−0.0002	0.0047	−0.0354	−0.0386	−0.1692
β_{yzz}	0.0002	−0.0003	−0.0002	0.0009	0.0021	−0.0027	−0.0049
β_{zzz}	−0.0003	−0.0006	0.0009	0.0007	0.0024	−0.0035	−0.0397
β_{tot}	0.8840	7.0440	3.9780	4.0880	3.9060	4.0090	4.1040

with ***p*-NA** revealed that all of the studied compounds displayed excellent NLO behavior.

(γ_{tot}) is a fundamental aspect for the determination of NLO properties.[80] Among all of the designed derivatives, the highest γ_{tot} value is also noted for **DTCM1** (14.68 × 10^{-32} esu). The decreasing order of γ_{tot} is as follows: **DTCM6** (22.260 × 10^{-34}) > **DTCM5** (5.148 × 10^{-34}) > **DTCM4** (3.348 × 10^{-34}) > **DTCM3** (0.858 × 10^{-34}) > **DTCM2** (0.320 × 10^{-34}) > **DTCM1** (0.063 × 10^{-34}) > **DTCMR** (0.249 × 10^{-34}). It can be observed that **DTCM6** exhibits the largest γ_x value of 22.260 × 10^{-34} esu among all of the investigated compounds and shows more charge shifting along the *x*-axis (Table 9). In conclusion, it has been examined that all of the designed compounds are polarizable and have a lesser band gap than **DTCMR**.

Table 9. Average Second Hyperpolarizability (γ_{tot} in esu) and Its Major Contributing Tensor Components Noticed for All Nominated Molecules

compounds	γ_x × 10^{-32}	γ_y × 10^{-33}	γ_z × 10^{-34}	γ_{tot} × 10^{-34}
DCTMR	9.096	1.651	3.332	0.249
DCTM1	14.340	3.352	2.721	0.063
DCTM2	7.154	6.054	2.257	0.320
DCTM3	9.006	2.799	2.651	0.858
DCTM4	9.216	1.365	2.925	3.348
DCTM5	9.810	1.723	1.042	5.148
DCTM6	11.140	1.615	0.680	22.260

Additionally, we also did a comparative study between our designed molecules and the data for **Compound 5**[81] and **DTPSD6**,[82] which have a similar structure to our designed structures (see Table 10). Our findings revealed significant improvements in both linear polarizability and second hyperpolarizability values compared to **Compound 5**. Specifically, the linear polarizability values of our derivatives were observed to be 6.11, 5.25, 5.29, 5.72, 6.02, 6.40, and 6.68 times greater than those of **Compound 5**. Similarly, the second hyperpolarizability values also showed improved results ranging from 6.049 to 54.29 times greater than those of compound **5**. Likewise, significant NLO behavior was also examined with **DTPSD6**; 1.65 to 1.80 times greater $\langle\alpha\rangle$ and 0.885 to 7.06 times greater β_{tot} response were investigated in our compounds than that of **DTPSD6**.

CONCLUSIONS

To explore the effect of extended π-conjugation (1*H*-pyrrole) on the nonlinear optical (NLO) properties, nonfullerene (NF)-based benzotrithiophene compounds (**DCTMR** and **DCTM1-DCTM6**) were designed. The effect of this structural tailoring in all of the designed molecules has been proficiently perceived for NLO response via DFT computations. The outcomes revealed that addition of the 1*H*-pyrrole unit had an encouraging impact on the D_1-π_1- D_2-π_2-A configuration and improved all of the properties of the fabricated compounds as compared to the reference molecule (**DCTMR**). The E_g of all of the derivatives is observed to be less (1.600−2.129 eV) than that of **DCTMR** along with a red shift. NBO findings revealed that prolonged conjugation improved the ICT process in chromophores. Additionally, GRP findings also explored a higher value of softness with a greater value of ΔN_{max} and smaller hardness in derivatives than that of **DCTMR**. These GRP findings supported the greater polarizability and CT in the fabricated chromophores; thus, magnificent NLO properties have been examined. Among all tailored chromophores, the highest β_{tot} and γ_{tot} were found for **DTCM1** and **DTCM6**, 7.0440 × 10^{-27} and 22.260 × 10^{-34} esu, respectively. It can be concluded that the incorporation of a polymeric unit (1*H*-pyrrole) in the molecular framework of all of the derivative molecules plays an important role in the fine-tuning of NLO properties. This research work would provide a deep understanding of the structure−property relationship with

Table 10. Comparison between the NLO Properties of the Above-Mentioned Compounds with Literature Data

our designed compounds				literature reported data				
compounds	$\langle\alpha\rangle$ × 10^{-22}	β_{tot} × 10^{-27}	γ_{tot} × 10^{-34}	compounds	$\langle\alpha\rangle$ × 10^{-22}	β_{tot} × 10^{-27}	γ_{tot} × 10^{-34}	refs
DCTMR	3.162	0.884	0.249	**compound 5**	0.510		0.041	81
DCTM1	2.715	7.044	0.063	**DTPSD6**	1.92	0.998		82
DCTM2	2.739	3.978	0.320					
DCTM3	2.958	4.088	0.858					
DCTM4	3.116	3.906	3.348					
DCTM5	3.308	4.009	5.148					
DCTM6	3.456	4.104	22.260					

https://doi.org/10.1021/acsomega.3c04774
ACS Omega 2023, 8, 39288−39302

the electronic properties. This work may also motivate experimental researchers to synthesize these compounds due to their significant NLO properties.

COMPUTATIONAL DETAILS

For this study, all of the computations were executed in chloroform utilizing the Gaussian 09 program.[83] For visualization and generating input data files, GaussView 6.0.16[84] software was used. First, geometrical optimization of all of the designed chromophores was accomplished at MPW1PW91[85] level of DFT[86] along with the 6-311G(d,p) basis set.[87] Time-dependent density functional theory (TD-DFT)[88] is an effective method in quantum chemistry to calculate the excitation energies because of its efficient and accurate results. Therefore, frontier molecular orbital (FMO) analysis, UV−vis study, global reactivity (GR), hole−electron interaction, density-of-states (DOS), and transition density matrix (TDM) were also performed at the aforesaid functional and basis sets by utilizing the TD-DFT approach. Other investigations: NLO and natural bond orbital (NBO) computations were achieved at the above-mentioned function of DFT. Gauss Sum,[89] Chem Craft 1.8,[90] Avogadro,[91] PyMOlyze 1.1,[92] Origin Lab,[93] GaussView 6.0.16,[84] and Multiwfn 3.8[94] software were utilized to interpret all of the results from the output files.

ASSOCIATED CONTENT

Data Availability Statement

Cartesian coordinates, UV−vis data (wavelengths, excitation energies and oscillator strengths), NBOs analysis, dipole moments, linear polarizabilities with major contributing tensors, the first hyperpolarizabilities (β_{tot}) and second hyperpolarizabilities (γ_{tot}) with their contributing tensors, ChemDraw structures and their IUPAC names and optimized geometries of the reported compounds were calculated using MPW1PW91/6-311G(d,p) and represented in Supporting data file.

Supporting Information

The Supporting Information is available free of charge at https://pubs.acs.org/doi/10.1021/acsomega.3c04774.

Cartesian coordinates of **DCTMR**; results of UV−vis absorption spectroscopy for **DCTMR** in solvent; natural bond orbitals (NBOs) analysis for **DCTMR** with its representative values; IUPAC names and abbreviations of investigated compounds (PDF)

AUTHOR INFORMATION

Corresponding Authors

Muhammad Adnan Asghar − *Department of Chemistry, Division of Science and Technology, University of Education Lahore, Lahore 54770, Pakistan;* orcid.org/0000-0003-0071-3580; Email: adnan.muhammad@ue.edu.pk

Suvash Chandra Ojha − *Department of Infectious Diseases, The Affiliated Hospital of Southwest Medical University, Luzhou 646000, China*; Email: suvash_ojha@swmu.edu.cn

Authors

Iqra Shafiq − *Institute of Chemistry, Khwaja Fareed University of Engineering & Information Technology, Rahim Yar Khan 64200, Pakistan; Centre for Theoretical and Computational Research, Khwaja Fareed University of Engineering & Information Technology, Rahim Yar Khan 64200, Pakistan*

Ayesha Mustafa − *Institute of Chemistry, Khwaja Fareed University of Engineering & Information Technology, Rahim Yar Khan 64200, Pakistan; Centre for Theoretical and Computational Research, Khwaja Fareed University of Engineering & Information Technology, Rahim Yar Khan 64200, Pakistan*

Romaisa Zahid − *Institute of Chemistry, Khwaja Fareed University of Engineering & Information Technology, Rahim Yar Khan 64200, Pakistan; Centre for Theoretical and Computational Research, Khwaja Fareed University of Engineering & Information Technology, Rahim Yar Khan 64200, Pakistan*

Rabia Baby − *Department of education, Sukkur IBA university, Sukkur 65200, Pakistan*

Sarfraz Ahmed − *Wellman Center for Photomedicine, Harvard Medical School, Massachusetts General Hospital, Boston, Massachusetts 02114, United States*

Tansir Ahamad − *Department of Chemistry, College of Science, King Saud University, Riyadh 11451, Saudi Arabia*

Manawwer Alam − *Department of Chemistry, College of Science, King Saud University, Riyadh 11451, Saudi Arabia*

Ataualpa A. C. Braga − *Departamento de Qu′ımica Fundamental, Instituto de Qu′ımica, Universidade de São Paulo, Sao Paulo 05508-000, Brazil;* orcid.org/0000-0001-7392-3701

Complete contact information is available at: https://pubs.acs.org/10.1021/acsomega.3c04774

Notes

The authors declare no competing financial interest.

ACKNOWLEDGMENTS

The authors are thankful to the Researchers Supporting Project (RSP2023R113), King Saud University, Riyadh, Saudi Arabia. The S.C.O. acknowledges the support from the doctoral research fund of the Affiliated Hospital of Southwest Medical University.

REFERENCES

(1) Sivasankari, B.; Roopan, S. M. L-Malic Acid-Doped Guanidinium Carbonate Crystal: A New NLO Material and Its Photoluminescence Study. *Optik* **2021**, *226*, No. 165909.

(2) Kosar, N.; Ayub, K.; Mahmood, T. Surface Functionalization of Twisted Graphene C32H15 and C104H52 Derivatives with Alkalis and Superalkalis for NLO Response; a DFT Study. *J. Mol. Graphics Modell.* **2021**, *102*, No. 107794.

(3) Vasumathi, S.; Jeyakumar, H. J.; Selvarajan, P. Spectral, NLO, Thermal, Hardness and SEM Studies of Phosphate Doped Bis-Urea Oxalic Acid Crystals for Laser Applications. *Chin. J. Phys.* **2021**, *73*, 1−12.

(4) Zhong, R.-L.; Xu, H.-L.; Muhammad, S.; Zhang, J.; Su, Z.-M. The Stability and Nonlinear Optical Properties: Encapsulation of an Excess Electron Compound LiCN··· Li within Boron Nitride Nanotubes. *J. Mater. Chem.* **2012**, *22* (5), 2196−2202.

(5) Ahsin, A.; Ayub, K. Remarkable Electronic and NLO Properties of Bimetallic Superalkali Clusters: A DFT Study. *J. Nanostruct. Chem.* **2021**, 1−17.

(6) Khan, B.; Khalid, M.; Shah, M. R.; Tahir, M. N.; Asif, H. M.; Aliabad, H. A. R.; Hussain, A. Synthetic, Spectroscopic, SC-XRD and Nonlinear Optical Analysis of Potent Hydrazide Derivatives: A Comparative Experimental and DFT/TD-DFT Exploration. *J. Mol. Struct.* **2020**, *1200*, No. 127140.

(7) Khan, M. U.; Khalid, M.; Ibrahim, M.; Braga, A. A. C.; Safdar, M.; Al-Saadi, A. A.; Janjua, M. R. S. A. First Theoretical Framework of Triphenylamine−Dicyanovinylene-Based Nonlinear Optical Dyes:

Structural Modification of π-Linkers. *J. Phys. Chem. C* **2018**, *122* (7), 4009−4018.
(8) Khalid, M.; Naz, S.; Mahmood, K.; Hussain, S.; Braga, A. A. C.; Hussain, R.; Ragab, A. H.; Al-Mhyawi, S. R. First Theoretical Probe for Efficient Enhancement of Optical Nonlinearity via Structural Modifications into Phenylene Based D−π−A Configured Molecules. *RSC Adv.* **2022**, *12* (48), 31192−31204.
(9) Khan, M. U.; Ibrahim, M.; Khalid, M.; Qureshi, M. S.; Gulzar, T.; Zia, K. M.; Al-Saadi, A. A.; Janjua, M. R. S. A. First Theoretical Probe for Efficient Enhancement of Nonlinear Optical Properties of Quinacridone Based Compounds through Various Modifications. *Chem. Phys. Lett.* **2019**, *715*, 222−230.
(10) Janjua, M. R. S. A.; Liu, C.-G.; Guan, W.; Zhuang, J.; Muhammad, S.; Yan, L.-K.; Su, Z.-M. Prediction of Remarkably Large Second-Order Nonlinear Optical Properties of Organoimido-Substituted Hexamolybdates. *J. Phys. Chem. A* **2009**, *113* (15), 3576−3587.
(11) Kanis, D. R.; Ratner, M. A.; Marks, T. J. Design and Construction of Molecular Assemblies with Large Second-Order Optical Nonlinearities. Quantum Chemical Aspects. *Chem. Rev.* **1994**, *94* (1), 195−242.
(12) Hurst, S. K.; Lucas, N. T.; Humphrey, M. G.; Asselberghs, I.; Van Boxel, R.; Persoons, A. Organometallic Complexes for Non-Linear Optics. XXVI. Quadratic Hyperpolarizabilities of Some 4-Methoxytetrafluorophenylalkynyl Gold and Ruthenium Complexes. *Aust. J. Chem.* **2001**, *54* (7), 447−451.
(13) Sivakumar, T.; Vignesh, S.; Jeyaperumal, K. S.; Muppudathi, A. L. Synthesis, Growth and Investigation of Structural, Optical, Photoluminescence and Thermal Studies on the ZnSO4-Doped DAST Crystal for NLO Applications. *J. Mater. Sci.: Mater. Electron.* **2021**, *32* (13), 17936−17945.
(14) Kim, S.-J.; Kang, B. J.; Puc, U.; Kim, W. T.; Jazbinsek, M.; Rotermund, F.; Kwon, O.-P. Highly Nonlinear Optical Organic Crystals for Efficient Terahertz Wave Generation, Detection, and Applications. *Adv. Opt. Mater.* **2021**, *9* (23), No. 2101019.
(15) Williams, D. J. Non-Linear Optical Properties of Organic Materials. *Thin Solid Films* **1992**, *216* (1), 117−122.
(16) Atalay, Y.; Avcı, D.; Başoğlu, A. Linear and Non-Linear Optical Properties of Some Donor−Acceptor Oxadiazoles by Ab Initio Hartree-Fock Calculations. *Struct. Chem.* **2008**, *19*, 239−246.
(17) Mahmood, R.; Janjua, M. R. S. A.; Jamil, S. DFT Molecular Simulation for Design and Effect of Core Bridging Acceptors (BA) on NLO Response: First Theoretical Framework to Enhance Nonlinearity through BA. *J. Cluster Sci.* **2017**, *28*, 3175−3183.
(18) Khalid, M.; Khan, M. U.; Shafiq, I.; Hussain, R.; Ali, A.; Imran, M.; Braga, A. A.; ur Rehman, M. F.; Akram, M. S. Structural Modulation of π-Conjugated Linkers in D−π−A Dyes Based on Triphenylamine Dicyanovinylene Framework to Explore the NLO Properties. *R. Soc. Open Sci.* **2021**, *8* (8), No. 210570.
(19) Lin, Y.; Zhan, X. Non-Fullerene Acceptors for Organic Photovoltaics: An Emerging Horizon. *Mater. Horiz.* **2014**, *1* (5), 470−488.
(20) Singh, S. P. Impact of End Groups on the Performance of Non-Fullerene Acceptors for Organic Solar Cell Applications. *J. Mater. Chem. A* **2019**, *7* (40), 22701−22729.
(21) Arshad, M. N.; Shafiq, I.; Khalid, M.; Asiri, A. M. Exploration of the Intriguing Photovoltaic Behavior for Fused Indacenodithiophene-Based A−D−A Conjugated Systems: A DFT Model Study. *ACS Omega* **2022**, *7* (14), 11606−11617.
(22) Duan, L.; Elumalai, N. K.; Zhang, Y.; Uddin, A. Progress in Non-Fullerene Acceptor Based Organic Solar Cells. *Sol. Energy Mater. Sol. Cells* **2019**, *193*, 22−65.
(23) Patra, D.; Park, S. Solution Processable Benzotrithiophene (BTT)-Based Organic Semiconductors: Recent Advances and Review. *Macromol. Rapid Commun.* **2022**, *43* (21), No. 2200473.
(24) Hou, J.; Park, M.-H.; Zhang, S.; Yao, Y.; Chen, L.-M.; Li, J.-H.; Yang, Y. Bandgap and Molecular Energy Level Control of Conjugated Polymer Photovoltaic Materials Based on Benzo [1, 2-b: 4, 5-B′] Dithiophene. *Macromolecules* **2008**, *41* (16), 6012−6018.
(25) Zhang, M.; Tsao, H. N.; Pisula, W.; Yang, C.; Mishra, A. K.; Müllen, K. Field-Effect Transistors Based on a Benzothiadiazole-Cyclopentadithiophene Copolymer. *J. Am. Chem. Soc.* **2007**, *129* (12), 3472−3473.
(26) Tsao, H. N.; Cho, D. M.; Park, I.; Hansen, M. R.; Mavrinskiy, A.; Yoon, D. Y.; Graf, R.; Pisula, W.; Spiess, H. W.; Müllen, K. Ultrahigh Mobility in Polymer Field-Effect Transistors by Design. *J. Am. Chem. Soc.* **2011**, *133* (8), 2605−2612.
(27) Beaujuge, P. M.; Pisula, W.; Tsao, H. N.; Ellinger, S.; Müllen, K.; Reynolds, J. R. Tailoring Structure- Property Relationships in Dithienosilole- Benzothiadiazole Donor- Acceptor Copolymers. *J. Am. Chem. Soc.* **2009**, *131* (22), 7514−7515.
(28) Wilson, L. J.; Klopfenstein, S. R.; Li, M. A Traceless Linker Approach to the Solid Phase Synthesis of Substituted Guanidines Utilizing a Novel Acyl Isothiocyanate Resin. *Tetrahedron Lett.* **1999**, *40* (21), 3999−4002.
(29) Irgashev, R. A.; Demina, N. S.; Rusinov, G. L. Construction of 2,3-Disubstituted Benzo[b]Thieno[2,3-d]Thiophenes and Benzo-[4,5]Selenopheno[3,2-b]Thiophenes Using the Fiesselmann Thiophene Synthesis. *Org. Biomol. Chem.* **2020**, *18* (16), 3164−3168.
(30) Ma, S.; Huang, Q.; Liang, Y.; Tang, H.; Chen, Y.; Zhang, J.; Zhang, K.; Huang, F.; Cao, Y. Non-Fullerene Electron Acceptors with Benzotrithiophene with π-Extension Terminal Groups for the Development of High-Efficiency Organic Solar Cells. *J. Mater. Chem. C* **2021**, *9* (39), 13896−13903.
(31) Khalid, M.; Lodhi, H. M.; Khan, M. U.; Imran, M. Structural Parameter-Modulated Nonlinear Optical Amplitude of Acceptor−π−D−π−Donor-Configured Pyrene Derivatives: A DFT Approach. *RSC Adv.* **2021**, *11* (23), 14237−14250.
(32) Ferdowsi, P.; Saygili, Y.; Zhang, W.; Edvinson, T.; Kavan, L.; Mokhtari, J.; Zakeeruddin, S. M.; Grätzel, M.; Hagfeldt, A. Molecular Design of Efficient Organic D−A—-A Dye Featuring Triphenylamine as Donor Fragment for Application in Dye-Sensitized Solar Cells. *ChemSusChem* **2018**, *11* (2), 494−502.
(33) Dai, X.; Dong, B.; Ren, M.; Lin, W. Unique D−π−A−π−D Type Fluorescent Probes for the Two-Photon Imaging of Intracellular Viscosity. *J. Mater. Chem. B* **2018**, *6* (3), 381−385.
(34) Peng, Z.; Yu, L. Second-Order Nonlinear Optical Polyimide with High-Temperature Stability. *Macromolecules* **1994**, *27* (9), 2638−2640.
(35) Amiri, S. S.; Makarem, S.; Ahmar, H.; Ashenagar, S. Theoretical Studies and Spectroscopic Characterization of Novel 4-Methyl-5-((5-Phenyl-1, 3, 4-Oxadiazol-2-Yl) Thio) Benzene-1, 2-Diol. *J. Mol. Struct.* **2016**, *1119*, 18−24.
(36) Nan, M. I.; Lakatos, E.; Giurgi, G.-I.; Szolga, L.; Po, R.; Terec, A.; Jungsuttiwong, S.; Grosu, I.; Roncali, J. Mono-and Di-Substituted Pyrene-Based Donor-π-Acceptor Systems with Phenyl and Thienyl π-Conjugating Bridges. *Dyes Pigm.* **2020**, *181*, No. 108527.
(37) Mahmood, A.; Abdullah, M. I.; Khan, S. U.-D. Enhancement of Nonlinear Optical (NLO) Properties of Indigo through Modification of Auxiliary Donor, Donor and Acceptor. *Spectrochim. Acta, Part A* **2015**, *139*, 425−430.
(38) Mishra, A. K.; Tewari, S. P. Density Functional Theory Calculations of Spectral, NLO, Reactivity, NBO Properties and Docking Study of Vincosamide-N-Oxide Active against Lung Cancer Cell Lines H1299. *SN Appl. Sci.* **2020**, *2*, 1−13.
(39) Zang, H.; Lou, J.; Jiao, S.; Li, H.; Du, Y.; Wang, J. Valorization of Chitin Derived N-Acetyl-D-Glucosamine into High Valuable N-Containing 3-Acetamido-5-Acetylfuran Using Pyridinium-Based Ionic Liquids. *J. Mol. Liq.* **2021**, *330*, No. 115667.
(40) de Siqueira Bezerra, Y. B.; de Oliveira, C. R. F.; Dornelles, L. P.; da Silva Guedes, C. C.; de Oliveira, A. P. S.; Coelho, L. C. B. B.; de Oliveira, C. H. C. M.; dos Santos, G. A.; Napoleão, T. H.; de Albuquerque Lima, T.; Paiva, P. M. G. Pesticidal Activity of Cratyllia Mollis Seed Lectin Preparation (Cramoll 1, 2, 3) against the Termite Nasutitermes Corniger and Mite Tetranychus Bastosi. *Crop Prot.* **2023**, *163*, No. 106093.

https://doi.org/10.1021/acsomega.3c04774
ACS Omega 2023, 8, 39288−39302

(41) Pearson, R. G. Absolute Electronegativity and Hardness Correlated with Molecular Orbital Theory. *Proc. Natl. Acad. Sci. U.S.A.* **1986**, *83* (22), 8440−8441.
(42) Kosar, B.; Albayrak, C. Spectroscopic Investigations and Quantum Chemical Computational Study of (E)-4-Methoxy-2-[(p-Tolylimino) Methyl] Phenol. *Spectrochim. Acta, Part A* **2011**, *78* (1), 160−167.
(43) Pearson, R. G. Absolute Electronegativity and Absolute Hardness of Lewis Acids and Bases. *J. Am. Chem. Soc.* **1985**, *107* (24), 6801−6806.
(44) Parr, R. G.; Yang, W. Density Functional Approach to the Frontier-Electron Theory of Chemical Reactivity. *J. Am. Chem. Soc.* **1984**, *106* (14), 4049−4050.
(45) Parr, R. G.; Donnelly, R. A.; Levy, M.; Palke, W. E. Electronegativity: The Density Functional Viewpoint. *J. Chem. Phys.* **1978**, *68* (8), 3801−3807.
(46) Parthasarathi, R.; Padmanabhan, J.; Elango, M.; Subramanian, V.; Chattaraj, P. K. Intermolecular Reactivity through the Generalized Philicity Concept. *Chem. Phys. Lett.* **2004**, *394* (4−6), 225−230.
(47) Parr, R. G.; Pearson, R. G. Absolute Hardness: Companion Parameter to Absolute Electronegativity. *J. Am. Chem. Soc.* **1983**, *105* (26), 7512−7516.
(48) Politzer, P.; Truhlar, D. G. Introduction: The Role of the Electrostatic Potential in Chemistry. *Chem. Appl. At. Mol. Electrost. Potentials* **1981**, 1−6.
(49) Chattaraj, P. K.; Roy, D. R. Update 1 of: Electrophilicity Index. *Chem. Rev.* **2007**, *107* (9), PR46−PR74.
(50) Pearson, R. G. Absolute Electronegativity and Hardness: Applications to Organic Chemistry. *J. Org. Chem.* **1989**, *54* (6), 1423−1430.
(51) Padmanabhan, J.; Parthasarathi, R.; Subramanian, V.; Chattaraj, P. K. Electrophilicity-Based Charge Transfer Descriptor. *J. Phys. Chem. A* **2007**, *111* (7), 1358−1361.
(52) Mulliken, R. S. A New Electroaffinity Scale; Together with Data on Valence States and on Valence Ionization Potentials and Electron Affinities. *J. Chem. Phys.* **1934**, *2* (11), 782−793.
(53) Koopmans, T. The Classification of Wave Functions and Eigen-Values to the Single Electrons of an Atom. *Physica* **1934**, *1* (1), 104−113.
(54) Maynard, A. T.; Huang, M.; Rice, W. G.; Covell, D. G. Reactivity of the HIV-1 Nucleocapsid Protein P7 Zinc Finger Domains from the Perspective of Density-Functional Theory. *Proc. Natl. Acad. Sci. U.S.A.* **1998**, *95* (20), 11578−11583.
(55) Parr, R. G.; Szentpály, Lv.; Liu, S. Electrophilicity Index. *J. Am. Chem. Soc.* **1999**, *121* (9), 1922−1924.
(56) Murmu, M.; Saha, S. K.; Guo, L.; Murmu, N. C.; Banerjee, P. Intrinsic Electronic Property and Adsorption of Organic Molecules on Specific Iron Surface: An Ab Initio DFT and DFTB Study. *J. Adhes. Sci. Technol.* **2022**, *37*, 1837−1855.
(57) Hao, R.; Li, Y.; Shan, S.; Xu, H.; Li, J.; Li, Z.; Li, R. Antioxidant Potential of Styrene Pyrone Polyphenols from Inonotus Obliquus: A Combined Experimental, Density Functional Theory (DFT) Approach and Molecular Dynamic (MD) Simulation. *J. Saudi Chem. Soc.* **2023**, *27*, No. 101652.
(58) Raja, M.; Muhamed, R. R.; Muthu, S.; Suresh, M. Synthesis, Spectroscopic (FT-IR, FT-Raman, NMR, UV−Visible), NLO, NBO, HOMO-LUMO, Fukui Function and Molecular Docking Study of (E)-1-(5-Bromo-2-Hydroxybenzylidene) Semicarbazide. *J. Mol. Struct.* **2017**, *1141*, 284−298.
(59) Pounds, A. J. Valency and Bonding: A Natural Bond Orbital Donor−Acceptor Perspective (Frank Weinhold and Clark Landis). *J. Chem. Educ.* **2007**, *84*, No. 43.
(60) Hussain, R.; Khan, M. U.; Mehboob, M. Y.; Khalid, M.; Iqbal, J.; Ayub, K.; Adnan, M.; Ahmed, M.; Atiq, K.; Mahmood, K. Enhancement in Photovoltaic Properties of N, N-Diethylaniline Based Donor Materials by Bridging Core Modifications for Efficient Solar Cells. *ChemistrySelect* **2020**, *5* (17), 5022−5034.
(61) Liu, Z.; Lu, T.; Chen, Q. An Sp-Hybridized All-Carboatomic Ring, Cyclo [18] Carbon: Electronic Structure, Electronic Spectrum, and Optical Nonlinearity. *Carbon* **2020**, *165*, 461−467.
(62) Ans, M.; Ayub, K.; Bhatti, I. A.; Iqbal, J. Designing Indacenodithiophene Based Non-Fullerene Acceptors with a Donor−Acceptor Combined Bridge for Organic Solar Cells. *RSC Adv.* **2019**, *9* (7), 3605−3617.
(63) Luzanov, A. V.; Sukhorukov, A. A.; Umanskii, V. E. Application of Transition Density Matrix for Analysis of Excited States. *Theor. Exp. Chem.* **1976**, *10*, 354−361.
(64) Lim, S. P.; Sheng, D. N. Many-Body Localization and Transition by Density Matrix Renormalization Group and Exact Diagonalization Studies. *Phys. Rev. B* **2016**, *94* (4), No. 045111.
(65) Sivakumar, G.; Paramasivam, M.; Bharath, D.; Rao, V. J. Energy Level Tuning of 'Z'-Shaped Small Molecular Non-Fullerene Electron Acceptors Based on a Dipyrrolo [2, 3-b: 2′, 3′-e] Pyrazine-2, 6 (1 H, 5 H)-Dione Acceptor Unit for Organic Photovoltaic Applications: A Joint Experimental and DFT Investigation on the Effect of Fluorination. *New J. Chem.* **2019**, *43* (13), 5173−5186.
(66) Lesar, A.; Milošev, I. Density Functional Study of the Corrosion Inhibition Properties of 1, 2, 4-Triazole and Its Amino Derivatives. *Chem. Phys. Lett.* **2009**, *483* (4−6), 198−203.
(67) Lakshminarayanan, S.; Jeyasingh, V.; Murugesan, K.; Selvapalam, N.; Dass, G. Molecular Electrostatic Potential (MEP) Surface Analysis of Chemo Sensors: An Extra Supporting Hand for Strength, Selectivity & Non-Traditional Interactions. *J. Photochem. Photobiol.* **2021**, *6*, No. 100022.
(68) Irfan, A.; Imran, M.; Khalid, M.; Ullah, M. S.; Khalid, N.; Assiri, M. A.; Thomas, R.; Muthu, S.; Basra, M. A. R.; Hussein, M.; et al. Phenolic and Flavonoid Contents in Malva Sylvestris and Exploration of Active Drugs as Antioxidant and Anti-COVID19 by Quantum Chemical and Molecular Docking Studies. *J. Saudi Chem. Soc.* **2021**, *25* (8), No. 101277.
(69) Iwan, A.; Sek, D. Polymers with Triphenylamine Units: Photonic and Electroactive Materials. *Prog. Polym. Sci.* **2011**, *36* (10), 1277−1325.
(70) Adant, C.; Dupuis, M.; Bredas, J. L. Ab Initio Study of the Nonlinear Optical Properties of Urea: Electron Correlation and Dispersion Effects. *Int. J. Quantum Chem.* **1995**, *56* (S29), 497−507.
(71) Morks, M. F. Magnesium Phosphate Treatment for Steel. *Mater. Lett.* **2004**, *58* (26), 3316−3319.
(72) Khalid, M.; Khan, M. U.; Shafiq, I.; Hussain, R.; Mahmood, K.; Hussain, A.; Jawaria, R.; Hussain, A.; Imran, M.; Assiri, M. A. NLO Potential Exploration for D−π−A Heterocyclic Organic Compounds by Incorporation of Various π-Linkers and Acceptor Units. *Arabian J. Chem.* **2021**, *14* (8), No. 103295.
(73) Margar, S. N.; Sekar, N. Nonlinear Optical Properties of Curcumin: Solvatochromism-Based Approach and Computational Study. *Mol. Phys.* **2016**, *114* (12), 1867−1879.
(74) Suresh, S.; Jayamoorthy, K.; Karthikeyan, S. Fluorescence Sensing of Potential NLO Material by Bunsenite NiO Nanoflakes: Room Temperature Magnetic Studies. *Sens. Actuators, B* **2016**, *232*, 269−275.
(75) Alparone, A. Linear and Nonlinear Optical Properties of Nucleic Acid Bases. *Chem. Phys.* **2013**, *410*, 90−98.
(76) Plaquet, A.; Guillaume, M.; Champagne, B.; Castet, F.; Ducasse, L.; Pozzo, J.-L.; Rodriguez, V. In Silico Optimization of Merocyanine-Spiropyran Compounds as Second-Order Nonlinear Optical Molecular Switches. *Phys. Chem. Chem. Phys.* **2008**, *10* (41), 6223−6232.
(77) Boyd, D. B.; Lipkowitz, K. B. *Reviews in Computational Chemistry*; John Wiley & Sons, 2009; Vol. *5*.
(78) Zaitri, L. K.; Mekelleche, S. M. Computational Study of Linear and Nonlinear Optical Properties of Substituted Thiophene Imino Dyes Using Long-Range Corrected Hybrid DFT Methods. *Mol. Phys.* **2020**, *118* (4), No. 1618508.
(79) Muhammad, S.; Shehzad, R. A.; Iqbal, J.; Al-Sehemi, A. G.; Saravanabhavan, M.; Khalid, M. Benchmark Study of the Linear and Nonlinear Optical Polarizabilities in Proto-Type NLO Molecule of

https://doi.org/10.1021/acsomega.3c04774
ACS Omega 2023, 8, 39288−39302

Para-Nitroaniline. *J. Theor. Comput. Chem.* **2019**, *18* (06), No. 1950030.
(80) Marks, T. J.; Ratner, M. A. Design, Synthesis, and Properties of Molecule-Based Assemblies with Large Second-Order Optical Nonlinearities. *Angew. Chem., Int. Ed. Engl.* **1995**, *34* (2), 155−173.
(81) Bibi, A.; Muhammad, S.; UrRehman, S.; Bibi, S.; Bashir, S.; Ayub, K.; Adnan, M.; Khalid, M. Chemically Modified Quinoidal Oligothiophenes for Enhanced Linear and Third-Order Nonlinear Optical Properties. *ACS Omega* **2021**, *6* (38), 24602−24613.
(82) Khalid, M.; Naseer, S.; Tahir, M. S.; Shafiq, I.; Munawar, K. S.; de Alcântara Morais, S. F.; Braga, A. A. A Theoretical Approach towards Designing of Banana Shaped Non-Fullerene Chromophores Using Efficient Acceptors Moieties: Exploration of Their NLO Response Properties. *Opt. Quantum Electron.* **2023**, *55* (3), No. 258.
(83) Frisch, M. J.; Clemente, F. R.; Frisch, Mj.; Trucks, Gw.; Schlegel, Hb.; Scuseria, Ge.; Robb, Ma.; Cheeseman, Jr; Scalmani, g.; Barone, V.; Mennucci, B.; Petersson, G. A.; Nakatsuji, H.; Caricato, M.; Li, X.; Hratchian, H. P.; Izmaylov, A. F.; Bloino, J.; Zhe, G. *Gaussian 09*, Revision a. 01, 2009.
(84) Dennington, R.; Keith, T. A.; Millam, J. M. *GaussView 6.0. 16*, Semichem Inc.; Shawnee Mission: KS, USA, 2016.
(85) Adamo, C.; Barone, V. Exchange Functionals with Improved Long-Range Behavior and Adiabatic Connection Methods without Adjustable Parameters: The m PW and m PW1PW Models. *J. Chem. Phys.* **1998**, *108* (2), 664−675.
(86) Lynch, B. J.; Truhlar, D. G. How Well Can Hybrid Density Functional Methods Predict Transition State Geometries and Barrier Heights? *J. Phys. Chem. A* **2001**, *105* (13), 2936−2941.
(87) Tsuzuki, S.; Uchimaru, T.; Mikami, M.; Tanabe, K. New Medium-Size Basis Sets to Evaluate the Dispersion Interaction of Hydrocarbon Molecules. *J. Phys. Chem. A* **1998**, *102* (12), 2091−2094.
(88) Marques, M. A.; Gross, E. K. Time-Dependent Density Functional Theory. *Annu. Rev. Phys. Chem.* **2004**, *55*, 427−455.
(89) O'boyle, N. M.; Tenderholt, A. L.; Langner, K. M. Cclib: A Library for Package-Independent Computational Chemistry Algorithms. *J. Comput. Chem.* **2008**, *29* (5), 839−845.
(90) Zhurko, G. A.; Zhurko, D. A. ChemCraft, Version 1.6 2009 http://www.chemcraftprog.com.
(91) Hanwell, M. D.; Curtis, D. E.; Lonie, D. C.; Vandermeersch, T.; Zurek, E.; Hutchison, G. R. Avogadro: An Advanced Semantic Chemical Editor, Visualization, and Analysis Platform. *J. Cheminf.* **2012**, *4* (1), 1−17.
(92) Tenderholt, A. L. *PyMOlyze*, Version 1.1.; Stanford University: CA Stanford, 2006.
(93) Stevenson, K. J. Review of Originpro 8.5. *J. Am. Chem. Soc.* **2011**, *133* (14), No. 5621.
(94) Lu, T.; Chen, F. Multiwfn: A Multifunctional Wavefunction Analyzer. *J. Comput. Chem.* **2012**, *33* (5), 580−592.

https://doi.org/10.1021/acsomega.3c04774
ACS Omega 2023, 8, 39288−39302